Optical and transport properties of piezoelectric [111]-oriented strained $Ga_{1-x}In_xSb/GaSb$ quantum wells

S. L. Wong, R. W. Martin, M. Lakrimi, R. J. Nicholas, T-Y. Seong, N. J. Mason, and P. J. Walker

Clarendon Laboratory, Oxford University, Parks Road, Oxford OX1 3PU, United Kingdom

(Received 18 February 1993; revised manuscript received 30 July 1993)

Magneto-optical and magnetotransport studies have been conducted on a series of strained single $Ga_{1-x}In_xSb/GaSb$ quantum wells grown along [001], [111]*A*, and [111]*B* directions by metal organic chemical vapor deposition. Both the interband transition energies and the two-dimensional carrier density show dramatic differences between the three orientations. Self-consistent calculations including the strain-induced piezoelectric field and the effect of band bending have been performed for the [111] structures. Results of the calculations agree very well with the observed dependences on indium content in the wells, well width, and cap thickness. The difference between [001] and [111] samples is due mainly to the presence of the piezoelectric field in the latter. The surface pinning field which is different in *both* direction and magnitude in the [111]*A* and [111]*B* structures contributes to the significant difference in these two orientations for cap thicknesses below 500 Å.

INTRODUCTION

There has been increasing interest in the study of [111]-oriented strained-layer zinc-blende semiconductor heterostructures. Smith and Mailhiot[1] predicted that due to the lack of inversion symmetry in such structures, large internal fields of the order of 10^5 V/cm will be generated by the strain. The in-built piezoelectric fields are sufficiently large to significantly alter the optical and electrical properties. Optical experiments[2–6] have confirmed the existence of strain-generated fields and the associated change in the confined energy levels. Utilization of this field for a blueshift self-electro-optic-effect device has been suggested and explored.[6] Theoretical predictions for application of such piezoelectric fields have also been made on the transport properties. A rearrangement of the internal charge profile to partially screen the piezoelectric field can be used to replace extrinsic doping[7] and to enhance carrier density and device performance.[8,9]

Recently, Martin *et al.* have reported magnetotransport results in piezoelectric [111]-oriented strained-layer $Ga_{1-x}In_xSb/GaSb$ quantum wells, showing two-dimensional carrier densities (N_{2D}) enhanced over those in corresponding [001] structures with differences observed between [111]*A* and [111]*B* orientations.[10] Since then, an enhanced N_{2D} has also been reported in strained [111] and [311] *n* and *p* channel $GaAs/Al_{1-x}Ga_xAs/In_{1-x}Ga_xAs$ structure.[11] Martin *et al.*[10] suggested qualitatively that the enhancement is due to a reorganization of charge induced by the internal electric field and that the surface pinning field, which is in the same (opposite) direction as the in-built field in the [111]*A*- ([111]*B*) -oriented well, produces the difference between these orientations.

In this paper, we report on the detailed quantitative results of self-consistent calculations for the [111] structures studied in Ref. 10. Both magnetotransport and magneto-optical measurements are also presented and compared with the theory. Our calculations clarify the systematic changes of N_{2D} obtained in the magnetotransport measurements and those of the interband transition energies in the magneto-optical studies as a function of well thickness, indium content of the well, cap thickness, and background doping level. This analysis provides a powerful means to control both the optical and transport properties in piezoelectric [111]-oriented strained quantum wells by independent variation of the growth parameters.

SAMPLE DETAILS

Strained single quantum wells of $Ga_{1-x}In_xSb/GaSb$ were simultaneously grown on [111]*A*-, [111]*B*-, and [001]-oriented GaAs substrates using atmospheric pressure metal organic chemical vapor deposition. The growth conditions were optimized for the [001] orientation as described earlier.[12] The $Ga_{1-x}In_xSb$ well is sandwiched between a GaSb capping layer, ranging from 100–2000 Å and a 2–4 μm GaSb buffer layer. The well thickness was varied from 40 to 120 Å. The samples are nominally undoped but are naturally *p* type due to residual acceptors ($\sim 10^{16}$ cm^{-3}) in the GaSb layers. The growth parameters are summarized in Table I for two series of samples, grown at different times. Magnetotransport and magneto-optical studies have been performed. Before considering the experimental details and results, we will present the self-consistent calculations on the [111] structures studied.

MODEL AND CALCULATION

Due to biaxial compression in the well, the heavy-hole and light-hole bands are split, with a type-II profile resulting for the light-hole band. Thus, in the figures and calculations, we have omitted the light hole for clarity.

TABLE I. The growth parameters and 4.2 K electrical properties of two series of quantum wells, showing differences between [001], [111]*A*, and [111]*B* orientations as a function of the cap thickness. All the wells nominally have 12% In content, with the exception of 881 which has 14%.

Sample number	Well width (Å)	Cap thickness (Å)	[001] p 10^{11} cm^{-2}	[001] μ m^2/V s	[111]*A* p 10^{11} cm^{-2}	[111]*A* μ m^2/V s	[111]*B* p 10^{11} cm^{-2}	[111]*B* μ m^2/V s
866	80	100	4.8	0.2	frozen out		6.7	0.6
869	80	260	2.1	0.7	frozen out		5.1	1.2
875	40	260	0.8	0.5	frozen out		3.4	0.3
885	80	260	1.2	1.0	frozen out		5.4	0.7
881	80	260	2.8	1.1	frozen out		7.8	1.0
880	120	260	1.5	0.9	frozen out		7.5	0.8
911	80	260	2.1	0.7	1.9	1.6	7.9	0.6
912	80	1040	1.7	0.3	2.5	0.8	2.1	0.6

N_{2D} and confinement energies of heavy hole and electron are found by numerically solving the Schrödinger and the Poisson equations self-consistently. We have taken into account the piezoelectric field and also the band bending in the well resulting from the accumulation of heavy holes from intrinsic p doping. For structures with thin capping layers, the effects of the surface have also been taken into account. Alloy parameters of $Ga_{1-x}In_xSb$ are taken from Ref. 13 and other physical constants from Ref. 14. The average valence-band offset is taken to be independent of strain and sample growth orientation from Ref. 15, which has been proved consistent with experimental results for this material combination.[16]

The schematic heavy-hole bands for the [001], [111]*A*, and [111]*B* samples for the thin cap case are shown in Fig. 1. For samples with a thick cap (> 1000 Å), the surface effect is negligible and the Fermi energy (E_F) is pinned at the acceptor level (E_A) of the GaSb bulk in both the cap and the buffer layer. In Fig. 1 the Fermi energy is pinned very close to the valence-band edge at the surface, as determined previously by measurements of the hole densities in a series of [001] GaSb/$Ga_{1-x}In_xSb$ quantum wells with cap thicknesses ranging from 100 Å to 2000 Å.[17] This surface pinning position of the Fermi level is due to a high concentration of surface acceptors, but the exact nature of these acceptors is not yet clear.

Due to the difference in biaxial strain direction between [001]- and [111]-oriented structures, the differences in the elastic strain tensors cause an orientation-dependent band-gap change and valence-band splitting. Taking [001] as the z direction, the strain tensors of the [001]- and [111]-oriented strained $Ga_{1-x}In_xSb$ well layer are, respectively, given by

$$\varepsilon_{xx}^{[001]}=\varepsilon_{yy}^{[001]}=\varepsilon_0\ ,\quad \varepsilon_{zz}^{[001]}=-\frac{2C_{12}}{C_{11}}\varepsilon_0\ , \tag{1}$$

$$\varepsilon_{ij}^{[001]}=0\quad (i,j=x,y,z,i\neq j)\ , \tag{2}$$

$$\varepsilon_{ii}^{[111]}=\frac{4C_{44}}{C_{11}+2C_{12}+4C_{44}}\varepsilon_0\quad (i=x,y,z)\ , \tag{3}$$

$$\varepsilon_{ij}^{[111]}=\frac{-(C_{11}+2C_{12})}{C_{11}+2C_{12}+4C_{44}}\varepsilon_0\quad (i,j=x,y,z,i\neq j)\ . \tag{4}$$

Here C_{11}, C_{12}, and C_{44} are the elastic constants, ε_0 is the lattice mismatch given by

$$\varepsilon_0=\frac{a_2}{a_1}-1\ , \tag{5}$$

where a_1 and a_2 are the lattice constants of $Ga_{1-x}In_xSb$ and GaSb, respectively. With Eqs. (1)–(4), we can calculate the strain-induced band-structure modifications for both orientations. The hydrostatic and shear deformation shifts, ΔE_H and ΔE_S, are given by[18]

$$\Delta E_{cH}^{[001]}=a_c(2\varepsilon_{xx}^{[001]}+\varepsilon_{zz}^{[001]}),\quad \Delta E_{cH}^{[111]}=3a_c\varepsilon_{ii}^{[111]}, \tag{6}$$

$$\Delta E_{vH}^{[001]}=a_v(2\varepsilon_{xx}^{[001]}+\varepsilon_{zz}^{[001]}),\quad \Delta E_{vH}^{[111]}=3a_v\varepsilon_{ii}^{[111]}, \tag{7}$$

$$\Delta E_S^{[001]}=2b(\varepsilon_{zz}^{[001]}-\varepsilon_{xx}^{[001]}),\quad \Delta E_S^{[111]}=2\sqrt{3}d\varepsilon_{ij}^{[111]}\ . \tag{8}$$

where a_c (a_v) is the conduction (valence) band hydrostatic deformation potential and b and d are the shear deformation potentials. The resulting band-gap change and valence band splitting can then be calculated. It is found that changing the growth direction from [001] to [111] does not produce much change in the heavy-hole depth (ΔE_{HH}) but more than halves the electron well depth (ΔE_C). It should be noted that although the average valence-band offset (or the *unstrained* band-offset ratio) is independent of orientation on the basis of *ab initio* pseudopotential calculations by Van de Walle and Martin,[19] the *strained* band-offset ratio is expected to be orientation dependent due to the orientation dependence of the band gap change caused by strain. Thus the $E1$ state in [111] structures is well above the lower barrier, being confined by the depletion field (surface field) in the buffer (cap) region in the [111]*A* ([111]*B*) orientation, whereas for [001], the $E1$ state is confined in the well.

The presence of off-diagonal strain components in the [111]-oriented wells also gives rise to an in-built field parallel to the [111] growth axis, $F^{[111]}$, given by

$$F^{[111]}=\frac{2\sqrt{3}e_{14}\varepsilon_{ij}^{[111]}}{\epsilon_0\epsilon_r}\ , \tag{9}$$

where ϵ_0, ϵ_r, and e_{14} are the permittivity of free space, the dielectric constant, and the piezoelectric constant of

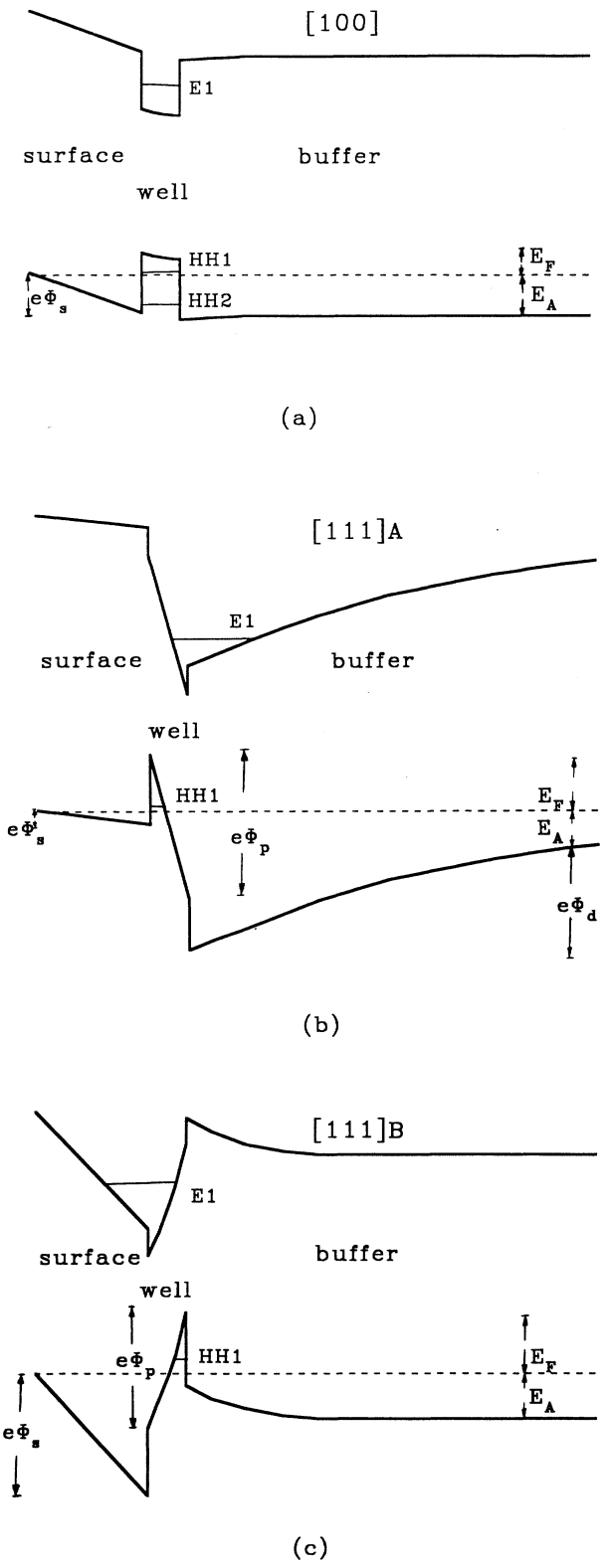

FIG. 1. Potential profiles for GaSb/$Ga_{1-x}In_xSb$ quantum wells in thin cap condition, for (a) [001], (b) [111]A, and (c) [111]B orientations. These are drawn based on the structures of 80 Å well width, 260 Å cap thickness, and 12% indium in the wells.

$Ga_{1-x}In_xSb$. Hence there is a field of order 10^5 V/cm across the well, in which the in-plane strain $\simeq -1.0\%$ (i.e., $\simeq 12\%$ indium). The potential drop across a typical well of width 80 Å and 12% In is about 87 meV and this is much greater than the heavy-hole well depth of 42 meV. Thus the potential profile in [111] samples is significantly altered, resulting in a dramatic change to the confined energy levels and their associated wave functions compared with their [001] equivalents. In changing from [001] to [111] orientation, the out-of-plane heavy-hole mass increases by about a factor of 2 due to the anisotropy of the valence band.[13] However, the resultant lowering of the confinement energy is far outweighed by the tilting of the band edge of the piezoelectric effect.

For a well under compression, the direction of the piezoelectric field points from the A (cation) to the B (anion) face, and is thus oppositely directed in the [111]A and [111]B samples. This results in very different characteristics in these two orientations for the thin cap case. In order to maintain E_F constant across the sample and to satisfy its pinning positions in the buffer and the surface, it is necessary to have very different surface fields and depletion fields in the buffer. The potential drop of the piezoelectric field, $e\Phi_p$, in the [111]A, ([111]B) structure is mainly balanced by the buffer depletion field, $e\Phi_d$ (surface field, $e\Phi_s$). The depletion field is due to the ionization of intrinsic acceptors in the thick buffer. The surface field results from both the ionization of intrinsic acceptors in the cap and surface acceptors states, with the latter being dominant. For a cap of 260 Å and an 80 Å well with 12% In, the surface field deduced self-consistently for a [111]B structure (see below) is of order 3×10^4 V/cm, which is equivalent to a surface charge density of $\sim 2.7\times10^{11}$ cm^{-2}. On the other hand, the surface field in [111]A structures is found to be close to zero so that there are negligible surface ionized acceptor states. Therefore, the band energy profile in the [111]A structure is very close to a thick cap condition. This explains the substantially enhanced N_{2D} in the [111]B over the [111]A structures and the different optical properties, which are seen for thin cap structures. In the qualitative picture of Ref. 10, this difference in magnitude of the surface field was not apparent.

The numerical calculation procedure starts by estimating the HH1 level in a triangular well potential, which results from the piezoelectric field in the absence of the band bending induced by the two-dimensional holes in the well, N_{2D}. Then the effect of N_{2D} is taken into consideration to give a new E_F (HH1$+E_{2D}$, where E_{2D} is the two-dimensional band filling energy). E_{2D} are related by the familiar expression

$$E_{2D}=\frac{\hbar^2\pi N_{2D}}{m_{HH}^{\parallel}}\ , \tag{10}$$

where $m_{HH}^{\parallel}$ is the in-plane mass. Instead of taking an energy dependent $m_{HH}^{\parallel}$ due to nonparabolicity, an average mass value of $0.1m_0$ is taken throughout. This simplification is supported by cyclotron resonance measurements for the [111]A structure of sample 911,[20] which show $m_{HH}^{\parallel}$ remaining close to $0.1m_0$ up to cyclo-

tron energy of 10 meV. It should be noted that $m_{HH}^{\parallel}$ depends on the degree of decoupling of the HH and LH bands, resulting from the strain, and a slight difference in the $m_{HH}^{\parallel}$ is therefore expected between samples with different indium content and well width. In the calculation, we have also ignored this small difference.

The N_{2D} value is adjusted until the resulting self-consistent potential profile of the heavy-hole band satisfies the relations

$$e\Phi_p = e\Phi_d - \Delta E_{HH} + E_F + E_A \tag{11}$$

for the [111]A structure and

$$e\Phi_p = e\Phi_s - \Delta E_{HH} + E_F \tag{12}$$

for the [111]B structure. The electron potential profile follows immediately from the final heavy-hole potential profile and the $E1$ state can then be found numerically. The interband transition energy is the sum of electron and heavy-hole confinement energies and the reduced band gap resulting from the tilting of the well.

Figures 2(a) and 2(b) show the calculated interband transition energies as a function of well width for a [111]B-oriented structure for the thin (260 Å) and thick (>1000 Å) cap conditions, respectively. A background doping level of 10^{16} cm^{-3} is assumed in the calculation as found in the growth of thick layers of bulk GaSb. Excitonic effects which are small in this system (the excitonic binding energy is of order of 3 meV from our magneto-optical measurements[16]) have not been considered in our calculations. As mentioned above, the results of the calculation in [111]A samples are very similar to the thick cap condition and are therefore not presented. Due to the highly asymmetric potential profile, originally forbidden $E1$-HH2 and $E1$-HH3 transitions are expected to become stronger in intensity as the overlap integrals increase. The theoretical values of N_{2D}, in units of 10^{11} cm^{-2}, are given in parentheses at the well widths indicated by arrows. As the well width increases, the potential drop across the well increases and results in the reduction of the band gap and hence the reduction in the interband transition energies. As seen in Fig. 1(b), for [111]A-oriented samples and samples with a thick cap (where surface field is negligible), any increase in $e\Phi_p$ produces a corresponding increase in $e\Phi_d$ in order to bring the Fermi level back to the acceptor level in the bulk. However, in the case of [111]B samples with a thin cap, as shown in Fig. 1(c), it is the potential energy due to the surface field, $e\Phi_s$, that increases in maintaining a constant E_F throughout the structure. Both the buffer depletion field and surface field result in an accumulation of ionized holes in the well. As the surface states generate a much higher concentration of holes in this thin cap [111]B structure, an enhanced N_{2D} results. This also leads to a stronger screening effect and is demonstrated by the smaller slopes in Fig. 2(a). HH2 and HH3 states are close in energy, lying just above the top of the lower barrier, and are effectively resonance continuum states instead of being confined.

Figure 3 shows the results of similar calculations as a function of the indium (In) content in the well. As the In content increases, so does the compressive strain in the well, resulting in a larger piezoelectric field. Furthermore, increasing the In content also decreases the alloy band gap of $Ga_{1-x}In_xSb$. The combined effect thus decreases the interband transition sharply. The difference in $E1$-HH1 and $E1$-HH2 energies increases as In increases. This provides a good test for the estimated In content in the well from the growth conditions. Again, smaller slopes are observed in Fig. 3(a) due to the stronger screening effect.

Figure 4 shows the results of calculations as a function of cap thickness in the [111]B structure. It demonstrates the dramatic enhancement of carrier density in the [111]B well as the cap thickness is reduced along with the observed blueshift of transition energies in the [111]B well compared with its [111]A counterpart for the thin cap case. The background doping level (N_A) also effects the observed optical and transport properties in the thick cap case and in the thin cap [111]A well as shown in Fig.

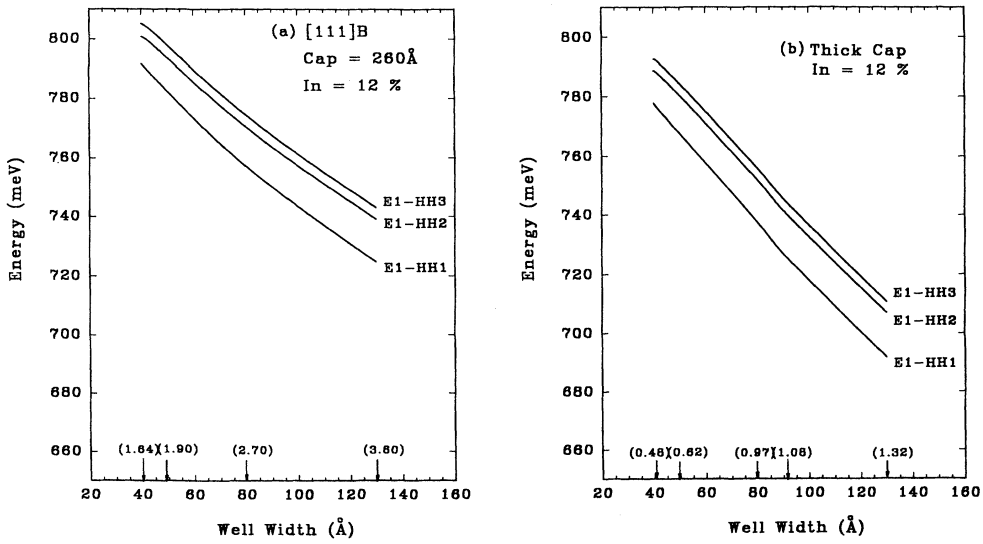

FIG. 2. Calculated interband transition energies as a function of well width for a [111]B-oriented structure with (a) thin cap of thickness 260 Å and (b) thick cap condition, respectively. The theoretical values of N_{2D}, in units of 10^{11} cm^{-2}, are given in parentheses at the well widths indicated by the arrows.

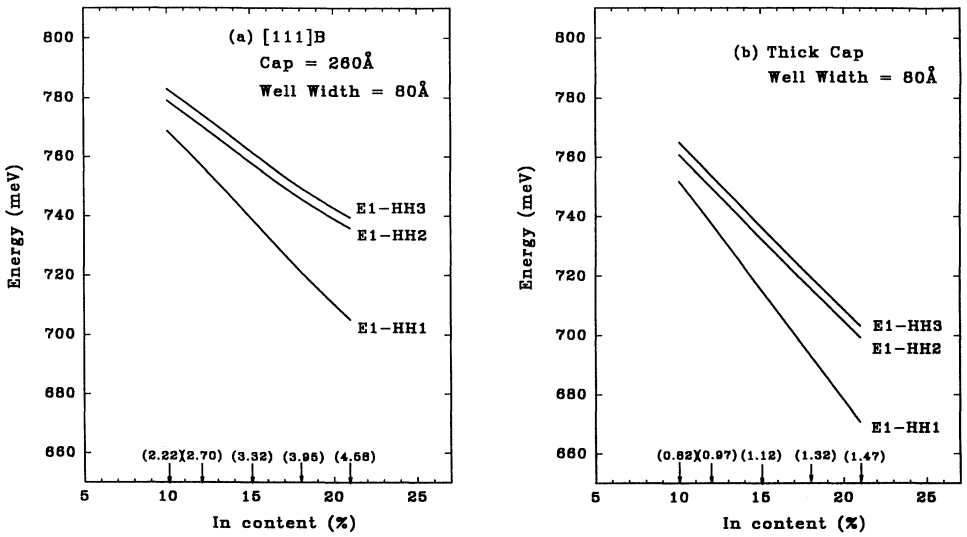

FIG. 3. As Fig. 2, but as a function of In content for a well of width 80 Å with a cap of thickness 260 Å.

5, although the effect is not as radical as the above three factors. N_A does not have much effect on thin cap [111]B samples since surface acceptor states have a dominant effect as mentioned before.

EXPERIMENTAL RESULTS AND DISCUSSION

Magnetotransport experiments were performed at temperatures down to 350 mK and magnetic fields up to 14.5 T, using a van der Pauw geometry. The experimental details have been given in Ref. 10 and a summary of the magnetotransport data is given in Table I. Transmission electron microscopy (TEM) measurements have been done on three samples (Table II), showing that the actual well and cap thicknesses of the [001] and [111]A samples are close to the nominal values while the [111]B sample has thicknesses less than the nominal ones. In addition, both [001] and [111]A samples show good morphology with the former having better quality while the [111]B sample shows considerable roughness. As described be-

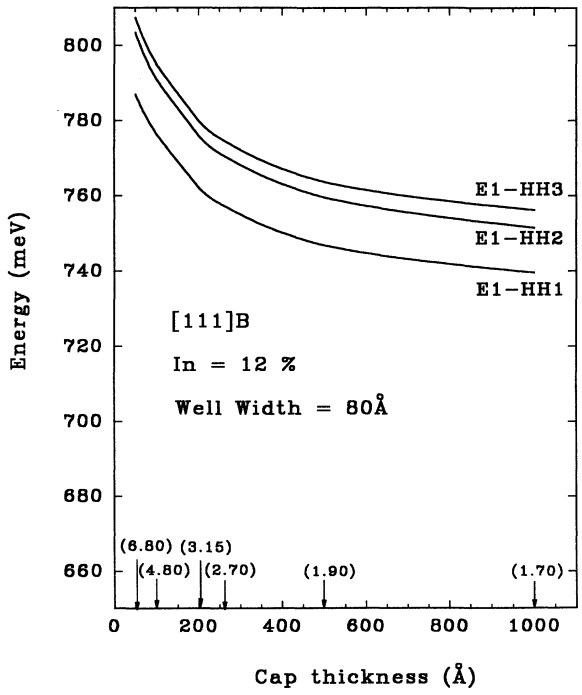

FIG. 4. Calculated interband transition energies as a function of cap thickness in the [111]B structure. The theoretical values of N_{2D}, in units of 10^{11} cm^{-2}, are given in parentheses at the cap thicknesses indicated by the arrows.

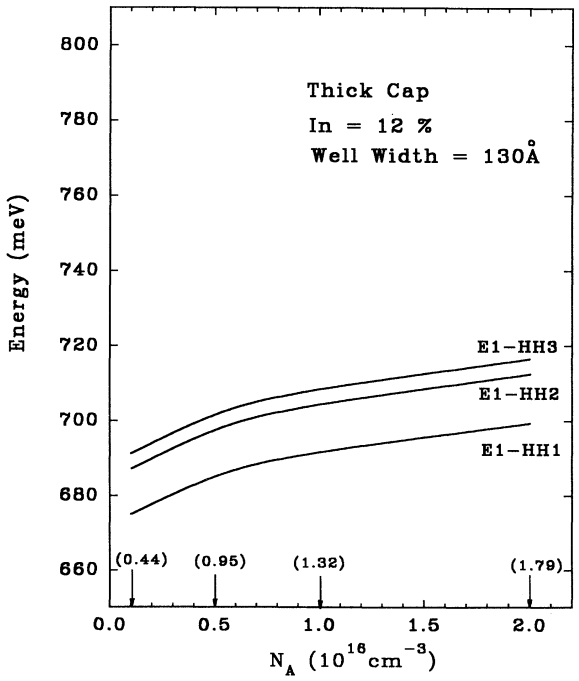

FIG. 5. Calculated interband transition energies as a function of background doping level in thick cap conditions. The theoretical values of N_{2D}, in units of 10^{11} cm^{-2}, are given in parentheses at the N_A indicated by the arrows.

TABLE II. Nominal and TEM measured well and cap thicknesses of three samples on which magneotphotoconductivity measurements have been performed. The wells nominally have 12% In content.

Sample	Orientation	Well (Å)		Cap (Å)	
		Nominal	Measured	Nominal	Measured
885	[001]	80	93±5	260	230±10
912	[111]*A*	80	83±10	1040	833±20
869	[111]*B*	80	65±25	260	110±30

fore, the growth conditions were optimized for the [001] orientation, and this indicates that the growth rate for [111]*B* structures is much slower under these conditions since the optimized growth conditions for [111]*B* structures are considerably different from those used in the simultaneous growth.

A different systematic behavior for the three orientations is observed. For thick cap layers, the [111]*A* and [111]*B* samples show comparable N_{2D} which are enhanced over those in the [001] samples. As the cap layer is made thinner, both [001] and [111]*B* structures show increased N_{2D}, while for [111]*A* there are no, or very few carriers. For both [111]*A* and [111]*B* structures, a gradual increase in N_{2D} is observed as the In content (well width) is increased. Using the mean well and cap thicknesses from the TEM result of sample 869 [111]*B*, and taking the In content to be 13% (as deduced from our magnetophotoconductivity results presented in the next paragraph), our self-consistent calculation gives an N_{2D} value of 4.5×10^{11} cm^{-2}. The effect of the decrease in the measured well thickness compared with the nominal value will reduce the N_{2D} while the opposite effect occurs for decreasing the cap thickness. The measured N_{2D} value of 5.1×10^{11} cm^2 indicates that the latter effect is slightly overcompensating the former, however the TEM results suggest that there may be macroscopic variations in the growth rates of the [111]*B* structures which may account for this small difference. The simplification of taking an energy independent in-plane hole mass may also lead to an underestimation of the N_{2D} value. This discrepancy should be more significant in thin cap [111]*B* structures, in which the HH band is filled up to a higher energy. Nevertheless, the experimentally observed trends for the carrier densities are well explained by the results of the above self-consistent calculations.

Magnetophotoconductivity measurements are performed at 4 K and magnetic fields up to 17 T to study the interband transition energies. Figure 6 shows the fan diagrams generated from the magnetophotoconductivity spectra of the three samples of Table II: (a) a nominal 260 Å cap [001] well, (b) a thick cap [111]*A* well, and (c) a nominal 260 Å cap [111]*B* well. The wells are nominally of width 80 Å and 12% In content. Obvious differences are observed in the three orientations. Figure 6(a) is a typical fan diagram of a conventional [001] structure with a clear *E*1-HH1 transition and associated Landau levels. Spin splitting is also resolved. Fitting of the transition energies using the envelope function approximation with Kane's **k·p** three-band model and inclusion of far band terms gives a well width of 92 Å with 11.5% In content in the well, which is in excellent agreement with the TEM results and nominal In content. A redshift of about 40 meV is observed for the [111]*A* samples [Fig. 6(b)] compared with its [001] counterpart. In addition to the *E*1-HH1 Landau level family, unresolved *E*1-HH2 and *E*1-HH3 states are also observed. Their strong oscillator strength is due to the highly asymmetric well potential profile. The difference between these unresolved transitions (*E*1-HH2 and *E*1-HH3) and *E*1-HH1 is about 15 meV. As found from our self-consistent calculation, this splitting is only sensitive to the In content. From Fig. 3(b), an In content of 12.3% will give rise to such a splitting. This is consistent with the nominal value. For this In content, Fig. 2(b) shows that a well width of 93 Å is required to give the observed transition energies, which is slightly larger than the nominal value and the value of the TEM measurement.

The fan diagram of the thin cap [111]*B* structure [Fig. 6(c)] is more complicated due to a higher hole density in the well, leading to both band filling effects and many-body band-gap renormalization. The transition energies are also higher up in energy so that masking by absorp-

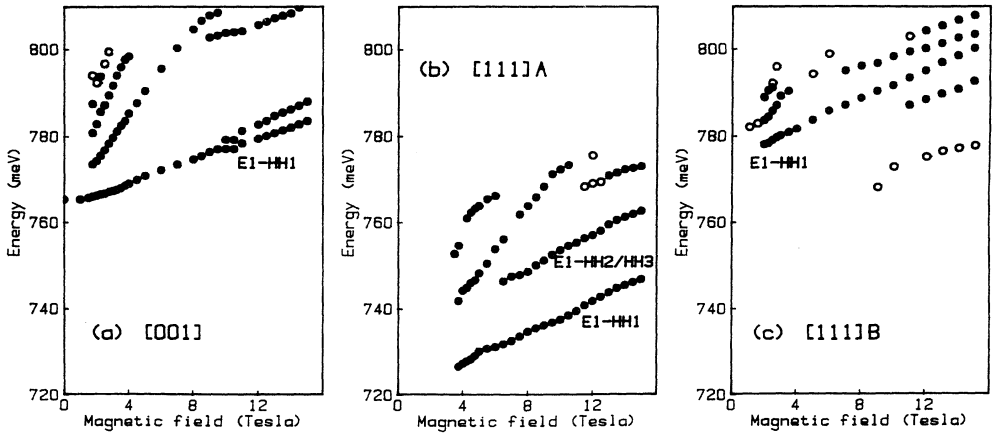

FIG. 6. Fan diagrams of (a) a nominal 260 Å cap [001] well, (b) a thick cap [111]*A* well, and (c) a nominal 260 Å cap [111]*B* sample. The wells are of width 80 Å and 12% In content nominally. Solid (open) circle are strong (weak) peaks from the magnetophotoconductivity spectra.

tion from the bulk GaSb transitions occurs above ~0.80 eV. Nevertheless, the fan diagram demonstrates an appreciable blueshift up to a quantum-well band gap of order 775 meV. This large blueshift in comparison with the [111]*A* structure is consistent with the theoretical predictions of Fig. 2 and Fig. 4, and the reduced well and cap thicknesses found by the TEM for the [111]*B* samples. With the mean well and cap thicknesses measured by TEM, an In content of 13% will give rise to an *E*1-HH1 transition of the observed value.

CONCLUSION

In summary, we have presented the results of self-consistent calculations on [111]-oriented $Ga_{1-x}In_xSb/GaSb$ wells, demonstrating the systematic relation of N_{2D} and interband transition energies. The results account very well for the observed trends in magnetotransport and magneto-optical measurements. This provides a powerful means of controlling the transport and the optical properties for device applications.

[1]D. L. Smith and C. Mailhiot, Rev. Mod. Phys. **62**, 173 (1990).
[2]B. K. Laurich, K. Elcess, C. G. Fonstad, J. G. Beery, C. Mailhiot, and D. L. Smith, Phys. Rev. Lett. **62**, 649 (1989).
[3]B. S. Yoo, X. C. Liu, A. Petrou, J-P. Cheng, A. A. Reeder, B. D. McCombe, K. Elcess, and C. Fonstad, Superlatt. Microstruct. **5**, 363 (1989).
[4]E. A. Caridi, T. Y. Chang, K. W. Goossen, and L. F. Eastman, Appl. Phys. Lett. **56**, 659 (1990).
[5]B. V. Shanabrook, D. Gammon, R. Beresford, W. I. Wang, R. P. Leavitt, and D. A. Broido, Superlatt. Microstruct. **7**, 363 (1990).
[6]K. W. Goossen, E. A. Caridi, T. Y. Chang, J. B. Stark, D. A. B. Miller, and R. A. Morgan, Appl. Phys. Lett. **56**, 715 (1990).
[7]E. S. Snow, B. V. Shanabrook, and D. Gammon, Appl. Phys. Lett. **56**, 758 (1990).
[8]J. Sànchez-Dehesa, J. L. Sànchez-Rojas, C. Lòpez, and R. J. Nicholas, Appl. Phys. Lett. **61**, 1072 (1992).
[9]U. Ekenberg and D. Richards, Surf. Sci. **263**, 580 (1992).
[10]R. W. Martin, M. Lakrimi, C. Lòpez, R. J. Nicholas, E. T. R. Chidley, N. J. Mason, and P. J. Walker, Appl. Phys. Lett. **59**, 659 (1991).
[11]X. Li, K. F. Longenbach, and W. I. Wang, Appl. Phys. Lett. **60**, 1513 (1992).
[12]S. K. Haywood, E. T. R. Chidley, R. E. Mallard, N. J. Mason, R. J. Nicholas, P. J. Walker, and R. J. Warburton, Appl. Phys. Lett. **54**, 922 (1989).
[13]A. P. Roth and E. Fortin, Can. J. Phys. **56**, 1468 (1978).
[14]*Numerical Data and Functional Relationships in Science and Technology*, edited by O. Madelung, Landolt-Börnstein, Group III, Vol. 17, Pt. a (Springer, New York, 1982).
[15]C. G. Van de Walle, Phys. Rev. B **39**, 1871 (1989).
[16]S. L. Wong, R. J. Warburton, R. J. Nicholas, N. J. Mason, and P. J. Walker, Physica B **184**, 106 (1993).
[17]M. Lakrimi, R. W. Martin, C. Lòpez, D. M. Symons, E. T. R. Chidley, R. J. Nicholas, N. J. Mason, and P. J. Walker, Semicond. Sci. Technol. **8**, S367 (1993).
[18]F. H. Pollak, Surf. Sci. **37**, 863 (1973).
[19]C. G. Van de Walle and R. M. Martin, Phys. Rev. B **34**, 5621 (1986).
[20]R. J. Warburton, R. A. Lewis, R. J. Nicholas, N. J. Mason, and P. J. Walker, Physica B **184**, 154 (1993).